URSI-RCRS 2024, ARIES/GEHU, Bhimtal, India, 22 - 25 October, 2024

The Role of Soil Moisture in Land-Atmosphere Interaction over North-East India Using Satellite Measurements and Modelling Approach

Aniket Chakraborty * (1), Binita Pathak (1), (2), Partha J. Sahu (2), Barlin Das (2) and Pradip K. Bhuyan (1)
(1) Centre for Atmospheric Studies, Dibrugarh University, India, 786004
(2) Department of Physics, Dibrugarh University, India, 786004

Abstract

The importance of soil moisture (SM) in land-atmosphere (L-A) interactions is significant because of its ability to influence surface heat fluxes and potentially have a positive feedback effect on parameters such as solar radiation, precipitation, and evaporative demand. Therefore, the study utilizes the AMSR-E (Advanced Microwave Scanning Radiometer-Earth Observing System), TMI (Tropical Rainfall Measuring Mission (TRMM) Microwave Imager), and SMAP (Soil Moisture Active Passive) satellite and reanalysis (IMDAA and ERA5-Land) datasets to establish the relation of SM with factors like latent heat flux (LHF), sensible heat flux (SHF), ground heat flux (GHF), planetary boundary layer (PBL) and relative humidity (RH) over North-East India (NEI). Further, an attempt was made with the WRF (Weather Research Forecasting) model by using the most suitable parameterization schemes to understand the credibility of the model in studying the above-mentioned relationships. The R-value between the SM measurements from IMDAA and AMSR-E/TMI/SMAP is found to be 0.79/0.78/0.76. From SMAP the LHF and SHF tend to have a positive and negative correlation (R-value) of 0.59 and -0.54 respectively with its SM measurements, whereas, GHF from SMAP is found to be neutral with its SM measurements (R-value ~ 0.03). Similarly, the SM measurement from IMDAA shows positive and negative correlation (R-value) of 0.89 and -0.54 for LHF and SHF, respectively. The R-value between IMDAA daytime SM and daytime PBL-height/RH is found to be -0.55/0.91. The WRF model could successfully simulate all the considered parameters having a relation with SM content except LHF, which struggles to maintain the positive correlation. Further, the SM simulated by the WRF model is highly correlated with the observed SMAP having an R-value of 0.86. Moreover, the RMSE (Root Mean Square Error) and MAE (Mean Absolute Error) were computed to be 2.35 and 2.08 respectively between the WRF model and observation, and the model underestimates the SMAP observation with the MBE (Mean Bias Error) of -1.43. The WRF model also manages to establish a negative correlation between its SM estimates and 2m air temperature (T2) having an R-value of -0.89.

1. Introduction

Interactions within the land-atmosphere (L-A) system are essential to the global cycles of energy and water. Thus, soil moisture (SM) affects not just the interactions between the air and the land but also the cycles of energy and water. It affects the near-surface air conditions and regulates the division of the total available energy into sensible heat fluxes (SHF) and latent heat fluxes (LHF) at the ground surface [1]. When there is a precipitation deficit, positive soil moisture–precipitation feedback can exacerbate heat and extend drought [2]. Thus, low SM causes a shift towards higher SHF by limiting surface LHF, which in turn leads to a partitioning of available energy into perceptible air heating [3]. As a result, the distribution of energy at the surface is altered, therefore the planetary boundary layer's (PBL) height changes by making it warmer and drier, and lowers the relative humidity (RH). The soil moisture-atmosphere feedback loop is strengthened even more by the shorter boundary layer's decreased capacity to transfer heat, moisture, and momentum upward. These variations in boundary layer dynamics, humidity, and surface energy partitioning caused by SM have significant effects on local to global weather, climate, and ecosystem processes [3].

Moreover, surface temperature, total cloud cover, and total water storage can all influence SM to some extent, either directly or indirectly. The total amount of cloud cover most likely has a dual effect on SM dynamics: it controls the input radiation energy on the surface that is directly related to the process of soil dry-down when there is no rainfall, and it frequently occurs at the same time as rainfall, which is associated with replenishing SM [4]. Earlier studies [5, 6] have shown the part of dry-air entrainment in upgrading surface dissipation and inducing a shallower convective boundary layer through daytime L-A feedback for the coupled L-A framework with practical daytime surface fluxes and atmospheric profiles. Evapotranspiration and surface energy partitioning are the main mechanisms that restrict the influence of SM on the near-surface temperature [7]. Wet soil and dry soil processes are the two primary forms of soil moisture feedback that may affect precipitation on convective periods, or diurnal time scales. When SM content is high, or when the soil is wet, there may be an increase in evapotranspiration and latent heat exchange with the atmosphere. Convective energy is often increased by these processes, even if the level of free convection (LFC) and lifting condensation level (LCL) tend to decrease. A rise in convective available potential energy (CAPE) and a decrease in LCL and LFC values can initiate deep convection, which can lead to rainfall [8, 9]. Conversely, dry soils increase sensible heat and the Bowen ratio, which increases LCL and LFC. While comparable dry soil mechanisms might impede deep convection if components cannot reach the LCL, strong sensible heating can assist reduce convective inhibition and eventually contribute to convection initiation and precipitation [10, 11].

These days, L-A interactions are better understood with the use of remote sensing datasets in terms of seasonal and yearly variability [12, 13]. Due to the limited coverage of in situ data, satellite remote sensing makes it possible to evaluate SM dynamics at the regional scale. Moreover, the utilisation of satellite data yields distinct information about SM that is unaffected by errors and possible bias present in model simulations [4]. The weather research and forecasting (WRF) model has several embedded options that may be used to produce land surface heat fluxes in numerical models at various resolutions [14]. The output of the model later be used directly to simulate the land surface heat fluxes, including the SHF and LHF [15].

In this study, we have examined the correlation between the SM and the other parameters related to L-A interaction over NEI using the SMAP satellite along with the IMDAA reanalysis and WRF model. Moreover, IMD gridded rainfall data has also been analysed parallelly with the SM measurements from AMSR-E and TRMM satellites and ERA5-Land reanalysis.

2. Methodology

2.1. Study Domain

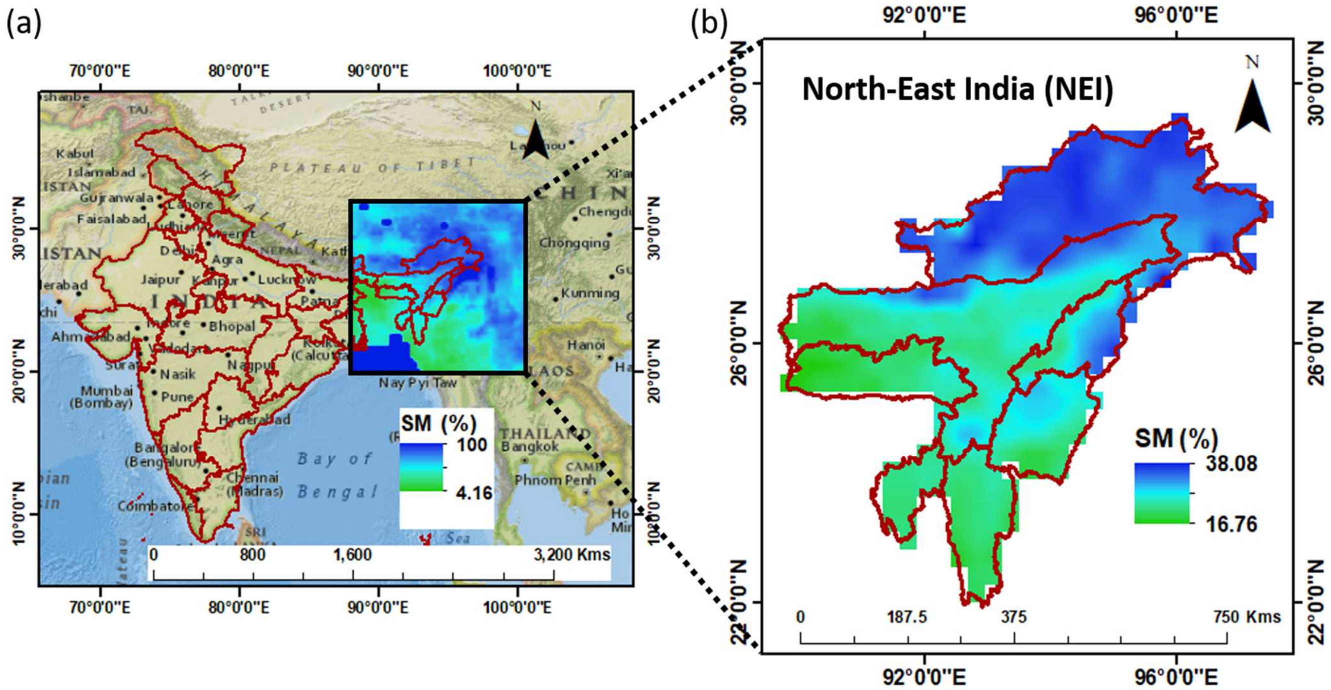

Figure 1. Spatial Map for the 16-day (11th May-26th May 2020) average volumetric soil moisture content **(a)** from the WRF model output representing the domain; and **(b)** representing the NEI (study region) clipped from the WRF model output.

North-East India (NEI) is stretched between 88°E and 98°E and 20°N and 30°N. The region is primarily hilly, with rocky terrain, alpine flora, and snow-capped high peaks dominating its physical features. According to climatology, the NEI has the least quantity of rainfall throughout the winter, making it the driest season of the year [16]. This area has a tropical monsoon climate, which is impacted by the way local topography and large-scale circulation interact. In this region, the predominant wind directions are mild north-easterlies in the winter, mild westerlies in the pre-monsoon, and strong westerlies in the monsoon. During post-monsoon months, there is comparatively less rainfall and calm, dry breezes. NEI is bounded by three international borders in all directions except the west, and it is physically isolated from the Indian mainland. Among the Himalayan states with extensive forested areas, the NEI is distinguished by a high proportion of rural inhabitants (72%) at a low population density (160 km^{-2}) and a general lack of infrastructure advancements. The population is heavily dependent on natural resources due to the significance of the major waterbodies (Brahmaputra and Barak rivers) and huge forest cover [17].

2.2. Data

Table: 1 Details of the data used.

Data Product	Data Portal	Spatial Resolution	Study Time Period	Description
IMD Rainfall	IMD Pune	0.25° x 0.25°	2002(July) - 2022	The daily measurements collected across India were used to approximate the monthly precipitation estimates. Rain gauge stations at about 6995 sites in India were used to quality-control rainfall records [18].
AMSR-E	GES DISC	25 km	2002(July) - 2011(September)	It utilised the volumetric water content estimations from the Level-3 surface soil moisture dataset, based on the Land Parameter Retrieval Model (LPRM) [19]. In this study, X-band ascending and descending AMSR-E retrievals are merged.
TMI	GES DISC	25 km	2011(October) - 2015(March)	Tropical Rainfall Measuring Mission (TRMM) Microwave Imager (TMI) soil moisture is reported twice daily as part of the TMI product, and volumetric water content is computed using the Land Parameter Retrieval Model from the TMI land surface temperature measurements [20].
SMAP	NSDIC	9 km	2015(March) - 2022(December)	Soil Moisture Active Passive (SMAP) satellite mission by the National Aeronautics and Space Administration (NASA) offers L-band brightness temperature data from descending and ascending half-orbit satellite passes (approximately 6:00 a.m. and 6:00 p.m. local solar time, respectively) are assimilated into a land surface model for each product [21].
ERA5-Land	Copernicus CDS	0.1° x 0.1°	1991 - 2020	Unlike ERA5, ERA5-Land is created independently of the atmospheric module of the ECMWF's integrated forecasting system (IFS), allowing for rapid updates without the need for data assimilation. SM estimates for four soil layers (i.e., 0–7, 7–28, 28–100, and 100–289 cm) with hourly temporal resolution are provided by ERA5-Land [22].
IMDAA (Indian Monsoon Data Assimilation and Analysis)	RDS NCMRWF	0.12° x 0.12°	1991 - 2020	The IMDAA system is based on the Met Office's four-dimensional variational assimilation method (4DVAR) and its Unified Model. The lateral boundary conditions for the analysis run are derived from the global reanalysis ERA-Interim [23].

2.3. WRF Model and Experiment Design:

The Unified Noah land-surface model [24] with multiparameterization options is used and linked with the widely utilised Weather Research and Forecasting (WRF) Model version 4.0, where the WRF preprocessing system (WPS v4.0) has been used for input preprocessing. The model domain is centred at 26.00°N and 94.00°E on a Mercator projection. It has 45 x 45 grid points in the east-west and north-south directions, respectively, with a horizontal resolution of 30 km × 30 km and 39 vertical levels from the surface up to 50 hPa. The simulated area is shown in Figure 1a and Table 2 consists of the list of different parameterization schemes that were chosen for this investigation. The first five days of the 21-day simulation period from 6th–26th May in the year 2020 are discarded for spin-up, and the rest of the 16-day outputs are used for the analysis. The period represents the pre-monsoon season when cyclone Amphan was generated in the Bay of Bengal (BoB) and hit Eastern India causing huge devastation, thus this period was chosen for the study purpose. The model's starting and boundary conditions were created using data from the Global Forecast System (GFS) of the National Centres for Environmental Prediction (NCEP) with 1° x 1° spatial and 6h temporal resolution, respectively (https://rda.ucar.edu/datasets/ds083.2/).

The model output has SM measurements for 4 layers and the study uses only the top layer i.e. the surface layer, just similar to the SM measurements considered from SMAP, IMDAA and ERA5-Land. The reason is that the effects of surface SM seem to be more immediate and noticeable than the deeper SM levels.

Table: 2 List of physical parameterizations used in the WRF Model.

Processes	Scheme
Bulk microphysical parameterization	Morrison 2-moment Scheme
Land surface	Unified Noah land-surface model
Planetary boundary layer (PBL)	Yonsei University Scheme, Mellor-Yamada-Janjic scheme
Shortwave radiation physics	Dudhia Shortwave Scheme
Longwave radiation physics	RRTM Longwave Scheme
Sf_sfclay_physics	Revised MM5 scheme
Cumulus parameterization	Grell 3D ensemble scheme

2.4. Statistical Analysis:

This study's statistical analysis includes the Pearson Correlation Coefficient (R-value), Mean Absolute Error (MAE), Root Mean Square Error (RMSE), and Mean Bias Error (MBE). Pearson Correlation (R-value) has been tested between IMD rainfall and all the satellite SM measurements, followed by the SM measurements between IMDAA and all other datasets. The linear relationship strength between the SM measurements from SMAP satellite observation and the WRF model across NEI is measured using the Pearson Correlation Coefficient (R-value). Besides that, the Model's performance is verified by the execution of RMSE, MAE, and MBE studies.

3. Results & Discussions

The primary source of SM is rainfall, and it is a dominant factor that influences the SM content in high-rainfall regions like NEI. Therefore, before establishing the relationship between SM and all other major L-A interaction parameters, it is necessary to understand the correlation of several SM products with rainfall measurements. Therefore, the most used IMD daily gridded rainfall data product is taken and processed into the monthly accumulated average rainfall for computing the correlation with the satellite SM measurements. The rainfall is considered for the same period July 2002 - December 2022, when SM satellite measurements are considered for the study (Figure 2).

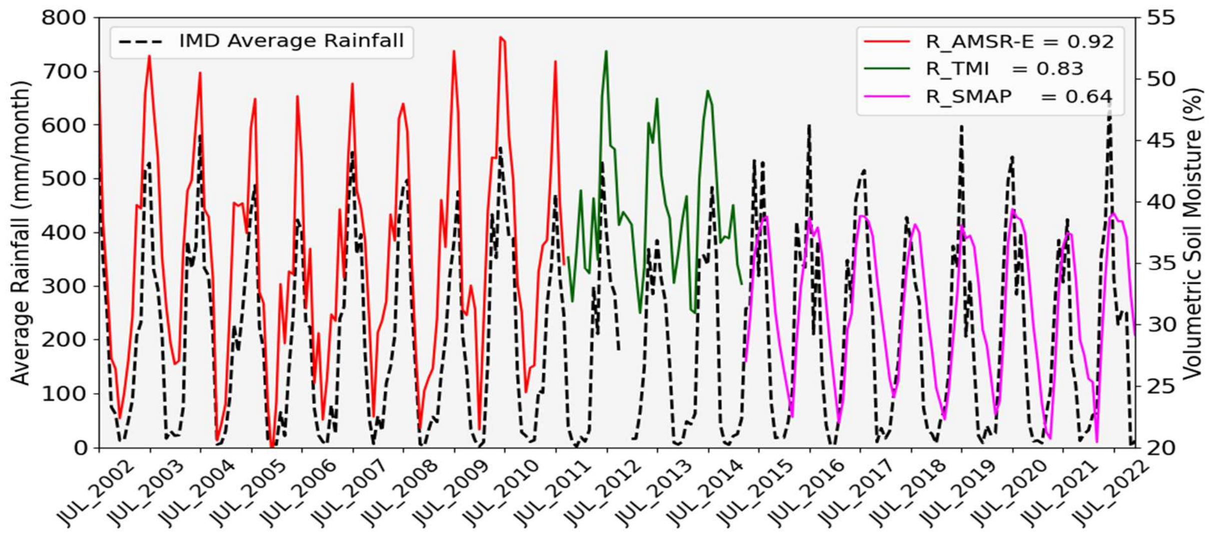

Figure 2. Monthly variation of average volumetric soil moisture measurements from AMSR-E, TMI and SMAP with the IMD average monthly rainfall.

The IMD rainfall and SM measurements from AMSR-E for July 2002 - September 2011 depict an R-value of 0.92. As AMSR-E ended in October 2011, AMSR2 was launched in May 2012 [25], as its successor. However, there is a gap of about 8 months, and thus the TMI retrieved SM product is chosen for the period October 2011 - March 2015 to maintain the continuation in SM data retrieval (Figure 2). Though TMI SM measurements and the IMD rainfall have an R-value of 0.83, still we have considered it for this small period as the high-resolution SM measurements from SMAP have been available from April 2015 till date. The L-band frequency (1.20-1.41 GHz) in SMAP is well-suited for SM sensing as it is sensitive to the dielectric properties of soil and can penetrate vegetation cover [26] which makes it the most important for SM measurements. The R-value for the SMAP SM and IMD rainfall is found to be 0.64 for April 2015 - December 2022.

By addressing the issues with sparse temporal and spatial distributions in data, the reanalysis products offer a more accurate estimate of SM than achieved from modelling or satellite observations alone. Reanalysis of SM offers distinct and reliable datasets for researching intricate spatial patterns of SM at regional, global, and temporal variability from hourly to yearly scales as well [27]. ERA5-Land reanalysis provides datasets globally and is preferred by many researchers, whereas, IMDAA is developed for the domain consisting of the Indian subcontinent. So, the correlation between the SM products from IMDAA and other satellite sensors along with ERA5-Land has been evaluated over the NEI region (Figure 3).

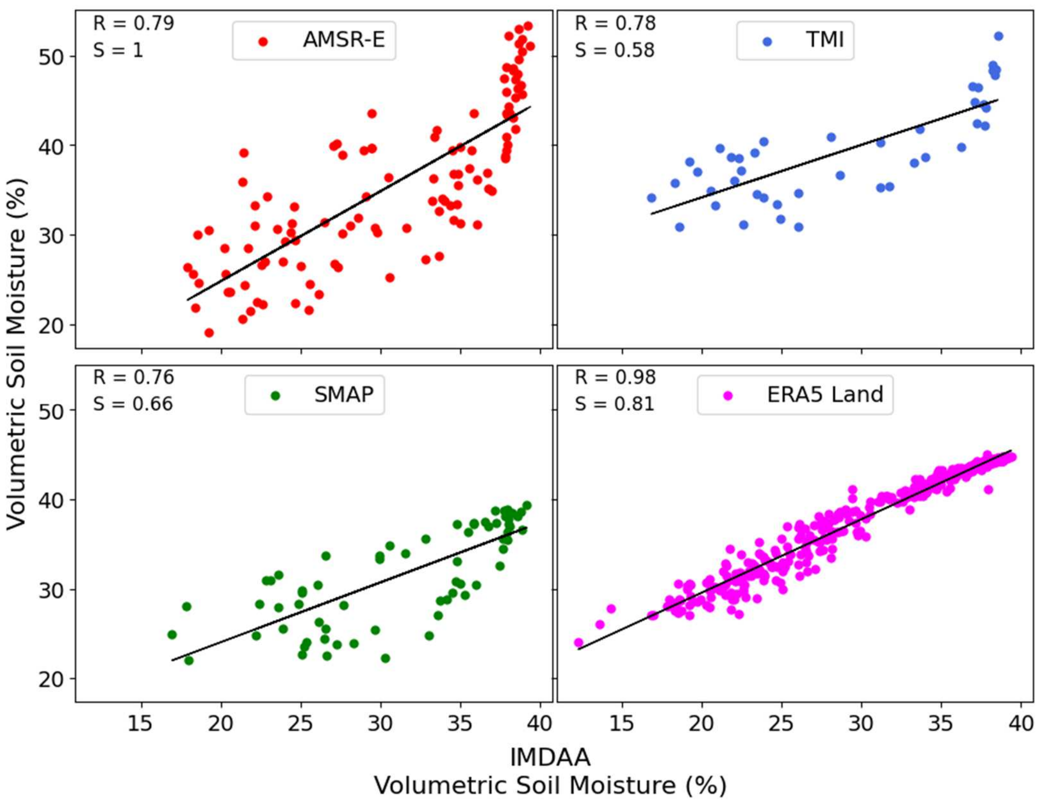

Figure 3. Scatter plot with regression fit depicting the correlations between SM measurements from IMDAA and SM measurements from AMSR-E, TMI, SMAP and ERA5-Land.

The study considered IMDAA and ERA5-Land for 3 decades (1991- 2020), and the correlation between SM from IMDAA and satellite measurements has been analysed for the respective considered period of the satellites. The R-value between the SM from IMDAA and AMSR-E/TMI/SMAP is found to be 0.79/0.78/0.76 for the period July 2002 - September 2011/ October 2011 - March 2015/ April 2015 - December 2022 (Figure 3). Further, the R-value of SM between IMDAA and ERA5-Land is found to be 0.98 from 1991 to 2020. Thus, the study suggests that due to this high correlation between IMDAA and ERA5-Land, they can be used interchangeably as reanalysis datasets. Moreover, the study reveals that satellite observations (AMSRE, TMI, and SMAP) and ERA5-Land are being underestimated by the IMDAA reanalysis instead of having a good positive correlation (Figure not shown).

As the study is focused mainly on establishing the relationship between SM and other L-A interacting parameters (LHF, SHF, GHF, PBL, and RH) over NEI, therefore the measurements from SMAP and IMDAA have been considered for 2016 to 2022 and 1991 to 2020 respectively (Figures 4 and 5). The monthly variations of these parameters over the years along with the SM have been presented in Figure 4. Moreover, the impact of SM on the other parameters is observed from the scatter plots depicting the correlation between SM and the other considered parameters from SMAP and IMDAA (Figure 5).

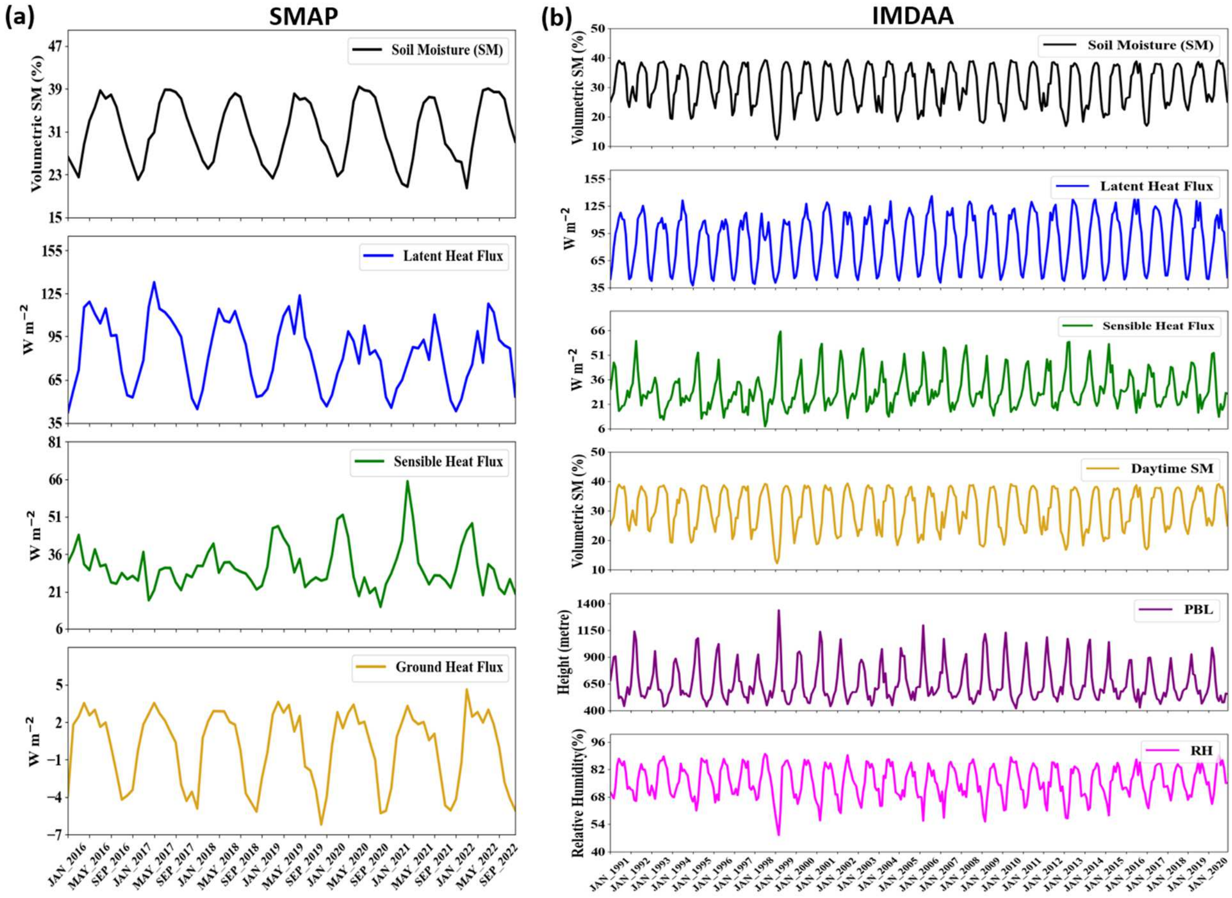

Figure 4. Line plot representing monthly **(a)** SM, LHF, SHF and GHF measurements from SMAP for NEI from 2016-2022 **(b)** SM, LHF, SHF, daytime PBL and daytime RH measurements from IMDAA reanalysis for NEI from 1991-2020.

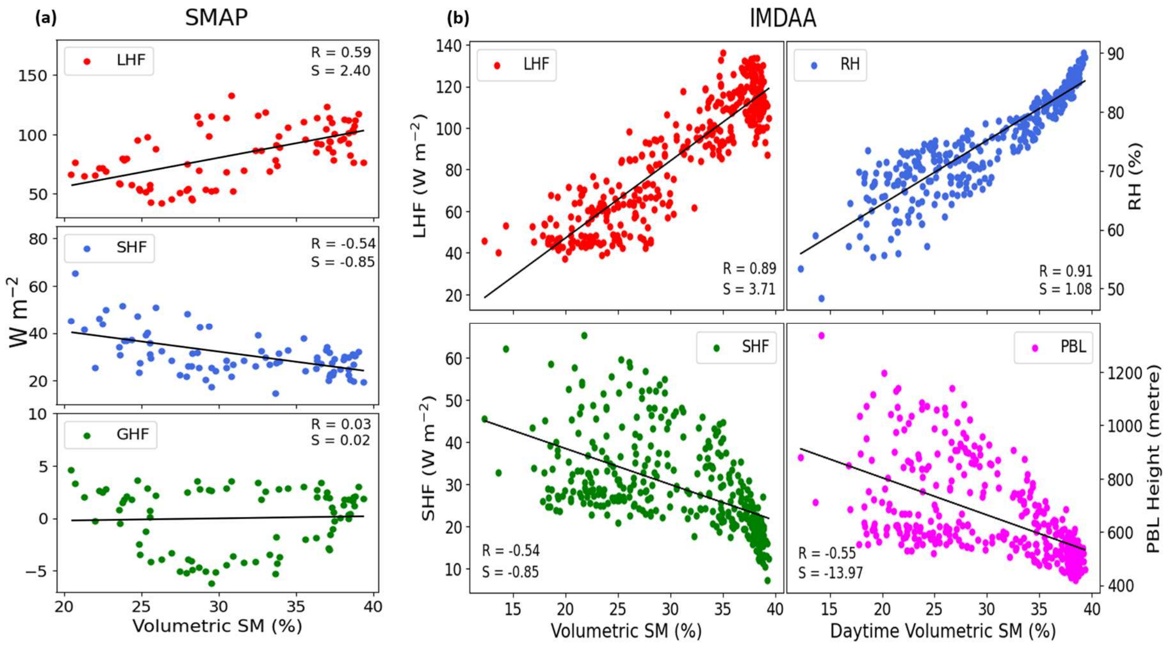

Figure 5. Scatter plot with regression fit depicting the correlation between SM and **(a)** LHF, SHF and GHF measurements from SMAP for NEI from 2016-2022 **(b)** LHF, SHF, daytime PBL and daytime RH measurements from IMDAA reanalysis for NEI from 1991-2020.

The material's transparency to sunlight is crucial for the computation of the Earth's surface energy balance. The conservation of energy at the L-A interface over land masses is stated as [28],

$$R_n = LHF + SHF + GHF \tag{1}$$

where R_n, LHF, SHF, and GHF are net radiation, latent, sensible, and ground heat fluxes, respectively. Positive radiative fluxes are those that reach towards the surface. LHF, SHF, and GHF entering the atmosphere and/or soil layer are defined as positive. Since SM directly controls the partitioning of surface energy fluxes between LHF and SHF, thus the relationship between SM and R_n is important feedback in the L-A interaction. As a result, SM affects the relative magnitudes of the energy balance components, including the GHF. SMAP provides the measurements regarding all the components that make the surface energy balance equation which further makes it important for this study (Figures 4a and 5a). As increased SM leads to a shallower PBL through enhanced LHF which also directly increases the RH in the surrounding air. Thus, it is important to study the nature of SM affecting PBL and RH, and to address it IMDAA dataset has been used (Figures 4b and 5b). From SMAP the LHF and SHF tend to have a positive and negative correlation (R-value) of 0.59 and -0.54 respectively with its SM measurements. Whereas, GHF from SMAP is found to be neutral with its SM measurements as the R-value is 0.03. Similarly, the SM measurement from IMDAA shows positive and negative correlation (R-value) of 0.89 and -0.54 for LHF and SHF, respectively. The PBL-height and the amount of RH in the atmosphere are mostly unstable during the daytime due to the stronger influence of surface heating, convection, and turbulent mixing. Therefore, only daytime (6 am to 3 pm) PBL-height, and RH measurements from IMDAA are considered along with daytime SM. The R-value is found to be -0.55 and 0.91 for daytime PBL-height and RH respectively, depicting daytime SM having a moderate-negative/ high-positive correlation with daytime PBL-height/RH.

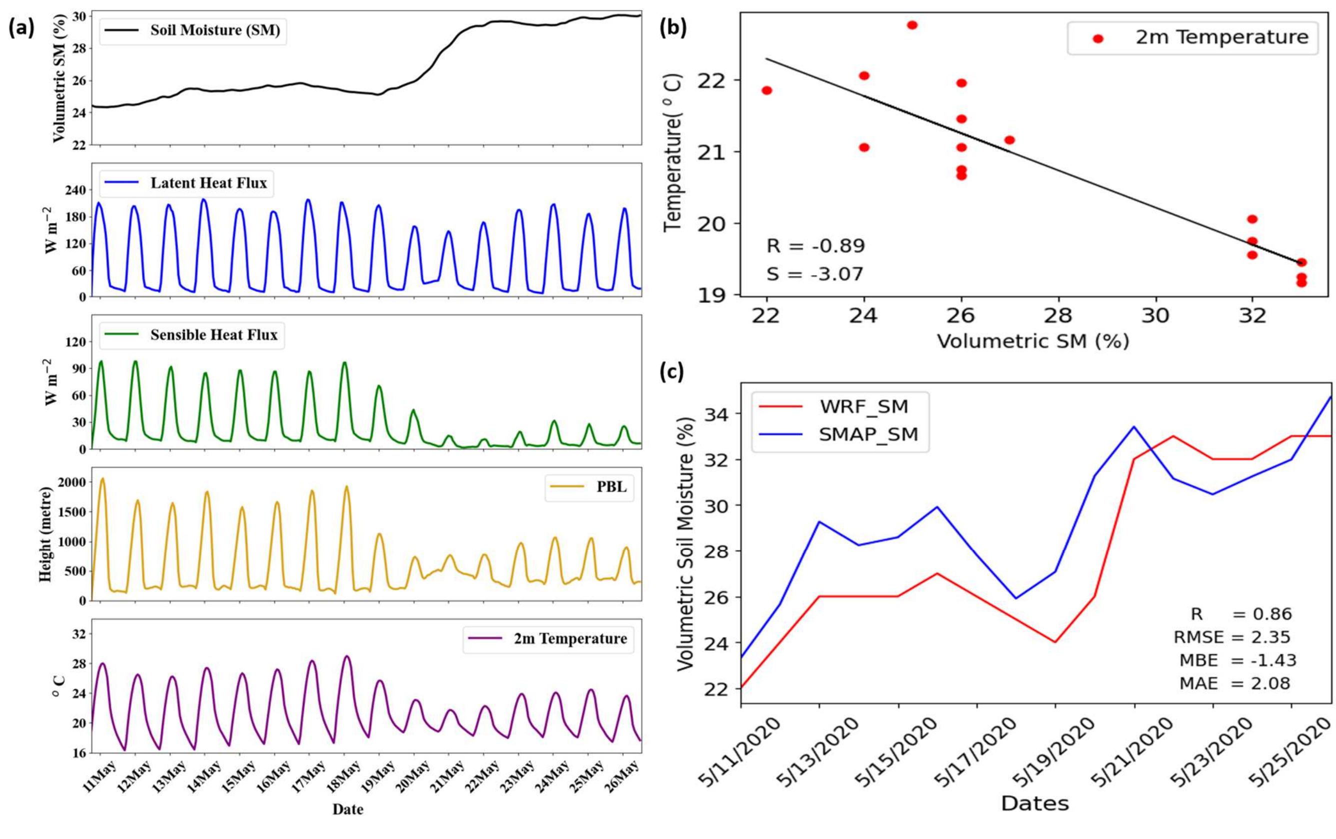

Figure 6. (a) Line plot showing diurnal variations of SM, LHF, SHF, PBL and T2 (2m air temperature) from WRF model output for NEI from 5:30 am 11th May to 11:30 pm 26th May 2020, **(b)** Scatter plot with regression fit depicting the relationship between SM and T2 from WRF model for NEI during 16 days, **(c)** line plots of average volumetric SM measurement from SMAP observation and estimates from WRF model for 16 days.

The study is further extended to use the WRF model to observe whether it could also establish a similar relationship between SM content and the other L-A interaction parameters over the NEI region. The details of the model setup have been discussed in the methodology section. Figure 6a depicts the diurnal variations of SM content, LHF, SHF, PBL-height, and the 2m air temperature (T2) from 5:30 am 11th May to 11:30 pm 26th May 2020. On critical observation, the SHF and PBL-height have shown a similar correlation with SM content as depicted by SMAP and IMDAA respectively, whereas the model struggles to maintain the positive correlation between LHF and SM as on 20th May the SM content starts increasing but the LHF got decreased and increased from 23rd May onwards. Interestingly, the WRF model could simulate T2 accordingly depicting a negative correlation (R-value) of -0.89 with SM content (Figure 6b) which goes in line with the other studies [29]. Lastly, it is mandatory to understand the performance of the WRF model where its average daily estimates of SM content are compared with the average daily SM observation from SMAP for the period 11th May to 26th May (Figure 6c). The WRF model depicts a high positive correlation (0.86) with the SMAP observation. The computed RMSE and MAE are 2.35 and 2.08 respectively. From Figure 6c itself, it can be stated that the WRF model underestimates the SMAP observation which is further strengthened by MBE analysis which is found to be -1.43.

4. Conclusions

In this study, the L-A interaction over the NEI region has been investigated where the relationship between SM and other factors like LHF, SHF, GHF, PBL, and RH is examined from satellite measurements, reanalysis, and the WRF numerical model. A similar relationship has been found in both satellite measurements (SMAP) and reanalysis (IMDAA) where LHF and SHF have positive and negative correlations (R-value) with SM respectively. Whereas, the PBL-height and RH from IMDAA depict negative and positive correlation respectively. The WRF model struggles with the LHF to maintain the existing positive correlation with the SM, which needs further model input parameterization fine-tuning. However, it well simulates the 2m air temperature according to the SM estimates with a high negative correlation, suggesting that low SM content can lead to increasing surface temperature. Thus, the study helps in understanding the intricate interactions between the Earth's surface and atmosphere through SM variations to understand the dynamics of L-A interaction, particularly in areas with diverse topography like NEI. Moreover, we can draw significant insights from a rigorous analysis of these relationships in NEI, with broad implications for climate modelling, weather forecasting, and sustainable land management in this ecologically delicate area.

5. Acknowledgements

The authors acknowledge IMD, NASA GES DISC, NSDIC, Copernicus CDS, and RDS NCMRWF for providing gridded rainfall data; AMSR-E, TMI; SMAP satellite measurements; ERA5-Land and IMDAA reanalysis datasets respectively. Aniket Chakraborty and Partha J Sahu acknowledge the ISRO-GBP-EOP project and ISRO-GBP-ARFI project respectively for providing fellowships. Binita Pathak acknowledges DST SERB for funding under the WEA scheme.

6. References

1. G. Seuffert, P. Gross, C. Simmer, and E. F. Wood, "The Influence of Hydrologic Modeling on the Predicted Local Weather: Two-Way Coupling of a Mesoscale Weather Prediction Model and a Land Surface Hydrologic Model," J. Hydrometeorol., vol. 3, no. 5, pp. 505–523, Oct. 2002, doi: 10.1175/1525-7541(2002)003<0505:TIOHMO>2.0.CO;2.

2. B. F. Zaitchik, J. A. Santanello, S. V. Kumar, and C. D. Peters-Lidard, "Representation of Soil Moisture Feedbacks during Drought in NASA Unified WRF (NU-WRF)," J. Hydrometeorol., vol. 14, no. 1, pp. 360–367, Feb. 2013, doi: 10.1175/JHM-D-12-069.1.

3. M. J. Alessi, D. A. Herrera, C. P. Evans, A. T. DeGaetano, and T. R. Ault, "Soil Moisture Conditions Determine Land‐Atmosphere Coupling and Drought Risk in the Northeastern United States," J. Geophys. Res. Atmospheres, vol. 127, no. 6, p. e2021JD034740, Mar. 2022, doi: 10.1029/2021JD034740.

4. K. Pangaluru et al., "Soil Moisture Variability in India: Relationship of Land Surface–Atmosphere Fields Using Maximum Covariance Analysis," Remote Sens., vol. 11, no. 3, p. 335, Feb. 2019, doi: 10.3390/rs11030335.

5. C. C. Van Heerwaarden, J. Vilà‐Guerau De Arellano, A. F. Moene, and A. A. M. Holtslag, "Interactions between dry‐air entrainment, surface evaporation and convective boundary‐layer development," Q. J. R. Meteorol. Soc., vol. 135, no. 642, pp. 1277–1291, Jul. 2009, doi: 10.1002/qj.431.

6. M. B. Ek and A. A. M. Holtslag, "Influence of Soil Moisture on Boundary Layer Cloud Development," J. Hydrometeorol., vol. 5, no. 1, pp. 86–99, Feb. 2004, doi: 10.1175/1525-7541(2004)005<0086:IOSMOB>2.0.CO;2.

7. E. B. Jaeger and S. I. Seneviratne, "Impact of soil moisture–atmosphere coupling on European climate extremes and trends in a regional climate model," Clim. Dyn., vol. 36, no. 9–10, pp. 1919–1939, May 2011, doi: 10.1007/s00382-010-0780-8.

9. J. S. Pal and E. A. B. Eltahir, "Pathways Relating Soil Moisture Conditions to Future Summer Rainfall within a Model of the Land–Atmosphere System," J. Clim., vol. 14, no. 6, pp. 1227–1242, Mar. 2001, doi: 10.1175/1520-0442(2001)014<1227:PRSMCT>2.0.CO;2.

9. J. A. Santanello, C. D. Peters-Lidard, and S. V. Kumar, “Diagnosing the Sensitivity of Local Land–Atmosphere Coupling via the Soil Moisture–Boundary Layer Interaction,” J. Hydrometeorol., vol. 12, no. 5, pp. 766–786, Oct. 2011, doi: 10.1175/JHM-D-10-05014.1.

10. C. M. Taylor et al., “Frequency of Sahelian storm initiation enhanced over mesoscale soil-moisture patterns,” Nat. Geosci., vol. 4, no. 7, pp. 430–433, Jul. 2011, doi: 10.1038/ngeo1173.

11. T. W. Ford, A. D. Rapp, and S. M. Quiring, “Does Afternoon Precipitation Occur Preferentially over Dry or Wet Soils in Oklahoma?,” J. Hydrometeorol., vol. 16, no. 2, pp. 874–888, Apr. 2015, doi: 10.1175/JHM-D-14-0005.1.

12. W. Dorigo et al., “Evaluating global trends (1988‐2010) in harmonized multi‐satellite surface soil moisture,” Geophys. Res. Lett., vol. 39, no. 18, p. 2012GL052988, Sep. 2012, doi: 10.1029/2012GL052988.

13. Y. Liu, W. Zhao, L. Wang, X. Zhang, S. Daryanto, and X. Fang, “Spatial Variations of Soil Moisture under Caragana korshinskii Kom. from Different Precipitation Zones: Field Based Analysis in the Loess Plateau, China,” Forests, vol. 7, no. 2, p. 31, Jan. 2016, doi: 10.3390/f7020031.

14. W. A. Gallus and J. F. Bresch, “Comparison of Impacts of WRF Dynamic Core, Physics Package, and Initial Conditions on Warm Season Rainfall Forecasts,” Mon. Weather Rev., vol. 134, no. 9, pp. 2632–2641, Sep. 2006, doi: 10.1175/MWR3198.1.

15. W. Ma and Y. Ma, “The evaluation of AMSR-E soil moisture data in atmospheric modeling using a suitable time series iteration to derive land surface fluxes over the Tibetan Plateau,” PLOS ONE, vol. 14, no. 12, p. e0226373, Dec. 2019, doi: 10.1371/journal.pone.0226373.

16. B. Pathak, P. K. Bhuyan, M. Gogoi, and K. Bhuyan, “Seasonal heterogeneity in aerosol types over Dibrugarh-North-Eastern India,” Atmos. Environ., vol. 47, pp. 307–315, Feb. 2012, doi: 10.1016/j.atmosenv.2011.10.061.

17. P. Dahutia, B. Pathak, and P. K. Bhuyan, “Aerosols characteristics, trends and their climatic implications over Northeast India and adjoining South Asia,” Int. J. Climatol., vol. 38, no. 3, pp. 1234–1256, Mar. 2018, doi: 10.1002/joc.5240.

18. D. S. Pai, M. Rajeevan, O. P. Sreejith, B. Mukhopadhyay, and N. S. Satbha, “Development of a new high spatial resolution (0.25° × 0.25°) long period (1901-2010) daily gridded rainfall data set over India and its comparison with existing data sets over the region,” MAUSAM, vol. 65, no. 1, pp. 1–18, Jan. 2014, doi: 10.54302/mausam.v65i1.851.

19. M. Owe, R. De Jeu, and T. Holmes, “Multisensor historical climatology of satellite‐derived global land surface moisture,” J. Geophys. Res. Earth Surf., vol. 113, no. F1, p. 2007JF000769, Mar. 2008, doi: 10.1029/2007JF000769.

20. H. Gao, E. F. Wood, T. J. Jackson, M. Drusch, and R. Bindlish, “Using TRMM/TMI to Retrieve Surface Soil Moisture over the Southern United States from 1998 to 2002,” J. Hydrometeorol., vol. 7, no. 1, pp. 23–38, Feb. 2006, doi: 10.1175/JHM473.1.

21. R. Reichle et al., “SMAP L4 Global 3-hourly 9 km EASE-Grid Surface and Root Zone Soil Moisture??Analysis Update, Version 7??” NASA National Snow and Ice Data Center Distributed Active Archive Center, 2022. doi: 10.5067/LWJ6TF5SZRG3.

22. Z. Wu, H. Feng, H. He, J. Zhou, and Y. Zhang, “Evaluation of Soil Moisture Climatology and Anomaly Components Derived From ERA5-Land and GLDAS-2.1 in China,” Water Resour. Manag., vol. 35, no. 2, pp. 629–643, Jan. 2021, doi: 10.1007/s11269-020-02743-w.

23. S. I. Rani et al., “IMDAA: High Resolution Satellite-era Reanalysis for the Indian Monsoon Region,” J. Clim., pp. 1–78, Mar. 2021, doi: 10.1175/JCLI-D-20-0412.1.

24. M. Tewari et al., “Implementation and verification of the unified NOAH land surface model in the WRF model.,” 2004, [Online]. Available: https://www2.mmm.ucar.edu/wrf/users/physics/phys_refs/LAND_SURFACE/noah.pdf

25. Q. Zhang, Q. Yuan, J. Li, Y. Wang, F. Sun, and L. Zhang, “Generating seamless global daily AMSR2 soil moisture (SGD-SM) long-term products for the years 2013–2019,” Earth Syst. Sci. Data, vol. 13, no. 3, pp. 1385–1401, Mar. 2021, doi: 10.5194/essd-13-1385-2021.

26. G. Singh, N. Das, R. Panda, B. Mohanty, D. Entekhabi, and B. Bhattacharya, “Soil Moisture Retrieval Using SMAP L-Band Radiometer and RISAT-1 C-Band SAR Data in the Paddy Dominated Tropical Region of India,” IEEE J. Sel. Top. Appl. Earth Obs. Remote Sens., vol. 14, pp. 10644–10664, 2021, doi: 10.1109/JSTARS.2021.3117273.

27. B. S. Naz, S. Kollet, H.-J. H. Franssen, C. Montzka, and W. Kurtz, “A 3 km spatially and temporally consistent European daily soil moisture reanalysis from 2000 to 2015,” Sci. Data, vol. 7, no. 1, p. 111, Apr. 2020, doi: 10.1038/s41597-020-0450-6.

28. S.-Y. Huang, Y. Deng, and J. Wang, “Revisiting the global surface energy budgets with maximum-entropy-production model of surface heat fluxes,” Clim. Dyn., vol. 49, no. 5–6, pp. 1531–1545, Sep. 2017, doi: 10.1007/s00382-016-3395-x.

29. C. Tang and D. Chen, “Interaction between Soil Moisture and Air Temperature in the Mississippi River Basin,” J. Water Resour. Prot., vol. 09, no. 10, pp. 1119–1131, 2017, doi: 10.4236/jwarp.2017.910073.